PNAS RESEARCH ARTICLE | CHEMISTRY

Metastable precipitation and ion–extractant transport in liquid–liquid separations of trivalent elements

Pan Sun[a,b,1,2], Xiao-Min Lin[c], Mrinal K. Bera[b], Binhua Lin[b], Dongchen Ying[d], Tieyan Chang[b], Wei Bu[b,1], and Mark L. Schlossman[a,1]

Edited by Shekhar Garde, Rensselaer Polytechnic Institute, Troy, NY; received September 7, 2023; accepted February 15, 2024 by Editorial Board Member Peter J. Rossky

The extractant-assisted transport of metal ions from aqueous to organic environments by liquid–liquid extraction has been widely used to separate and recover critical elements on an industrial scale. While current efforts focus on designing better extractants and optimizing process conditions, the mechanism that underlies ionic transport remains poorly understood. Here, we report a nonequilibrium process in the bulk aqueous phase that influences interfacial ion transport: the formation of metastable ion–extractant precipitates away from the liquid–liquid interface, separated from it by a depletion region without precipitates. Although the precipitate is soluble in the organic phase, the depletion region separates the two and ions are sequestered in a long-lived metastable state. Since precipitation removes extractants from the aqueous phase, even extractants that are sparingly soluble in water will continue to be withdrawn from the organic phase to feed the aqueous precipitation process. Solute concentrations in both phases and the aqueous pH influence the temporal evolution of the process and ionic partitioning between the precipitate and organic phase. Aqueous ion–extractant precipitation during liquid–liquid extraction provides a reaction path that can influence the extraction kinetics, which plays an important role in designing advanced processes to separate rare earths and other minerals.

solvent extraction | lanthanides | rare earth elements | liquid interfaces | precipitate depletion

Significance

The chemical process of liquid–liquid extraction is widely used to mine, recycle, separate, and purify critical elements such as rare earths, as well as treat nuclear waste. During this process that takes place in two-phase aqueous/organic systems, third phases and precipitates may form that spoil the quality and efficiency of the process. Most studies of such third phases and precipitates have focused on the organic phase. Here, we present experiments that provide a deeper understanding of how precipitation may occur in the aqueous phase and compete kinetically with the intended transport of rare earth elements into the organic phase. This understanding may lead to developments that enhance the separation and purification of critical elements.

Ion transport through interfaces between immiscible fluids underlies the separation of a wide range of elements and molecules that are important in the areas of biology, high-tech manufacturing, and environmental remediation (1–4). Solvent extraction is a common separation process in which target ions, often metallic, are selectively extracted from a complex aqueous mixture into an organic phase. Organic-soluble extractants assist the selective transport of metal ions by complexing with them and enhancing their solubility in the organic phase. Complexation is believed to take place either at the liquid–liquid interface, where slightly amphiphilic extractants gather, or in the aqueous boundary layer near the interface, where extractants that are slightly soluble in the aqueous phase can be found (5–9). Evidence for ion–extractant complexation at liquid interfaces, including the liquid–liquid interface, comes from X-ray and neutron scattering studies, as well as from nonlinear optical studies of organic–aqueous and aqueous–vapor interfaces (10–18). Evidence that ion–extractant complexation can also take place in the aqueous boundary layer has relied upon models for the kinetics of extraction, which is important for their practical application (8, 9, 19). The kinetics of extraction will be different if extractants react directly with ions at the organic–aqueous interface or if extractants pass through the interface and diffuse within the aqueous phase before reacting with ions.

Recent investigations have also provided evidence that the location of ion–extractant reactions, either at the interface or in the aqueous phase, can affect the selectivity of the extractant process, that is, the preferential extraction of one ionic species over another (18, 20). These investigations explored the effect of lanthanide ion–extractant complexation within a bulk aqueous phase on the presence of ions at the water-vapor interface in the absence of an organic phase (18, 20). Ions that interacted more strongly with soluble extractants were less likely to be found at the water-vapor interface. Instead, they formed ion–extractant complexes that were solubilized in the bulk aqueous phase. However, if the extractants were confined to the water-vapor interface, then the more strongly interacting ions would be found preferentially at the interface. These results suggested that the common expectation that a stronger ion–extractant interaction will lead to preferential extraction relied upon ions and extractants interacting directly at the interface. However, the practical consequences of aqueous complexation on selectivity might be expected to be small or relevant only in special situations for most extractants because their solubility in aqueous phases is much lower than in organic phases.

Author contributions: P.S., W.B., and M.L.S. designed research; P.S., X.-M.L., M.K.B., B.L., D.Y., T.C., and W.B. performed research; P.S., M.K.B., W.B., and M.L.S. analyzed data; and P.S., M.K.B., B.L., W.B., and M.L.S. wrote the paper.

The authors declare no competing interest.

This article is a PNAS Direct Submission. S.G. is a guest editor invited by the Editorial Board.

[1]To whom correspondence may be addressed. Email: psun20@uic.edu, weibu@uchicago.edu, or schloss@uic.edu.

[2]Present Address: Chemical Sciences Division, Oak Ridge National Laboratory, Oak Ridge, TN 37831.

This article contains supporting information online at https://www.pnas.org/lookup/suppl/doi:10.1073/pnas.2315584121/-/DCSupplemental.

Published March 20, 2024.

The concentration of extractants in these recent studies was limited by their low solubility in the aqueous phase, but also by the design of the studies which arranged for the concentrations to be well below saturation, roughly 10% of saturation, to avoid any instabilities produced by evaporation that might have occurred during the measurements (18, 20). Industrial solvent extraction processes, however, benefit from an organic solution of extractants, often at high concentration, that acts as a reservoir to supply extractants to the liquid–liquid interface or to the aqueous phase (21). Sometimes, the high concentration produces a third phase in equilibrium with the organic and aqueous phases, a Winsor microemulsion consisting of oil, water, ions, and extractants, that appears between the organic and aqueous phases (22–25). Solid phases are also known to form at the interface, commonly referred to as interfacial crud (26, 27). Solid phases or precipitates have been observed in aqueous phases in centrifugal contractors used in, for example, spent nuclear fuel processing (28). Microemulsion third phase formation, cruds, and precipitates are well known in industrial applications of solvent extraction, where processes are usually designed to avoid their formation due to the difficulty of further processing the ions contained within them (28–30).

Here, we explore the role of bulk aqueous complexation of ions and extractants when it leads to aqueous phase precipitation, which is distinct from the formation of microemulsion phases or precipitation at the aqueous-organic solvent interface. This research provides a deeper understanding of how precipitation may occur in the aqueous phase and compete kinetically with extractant-assisted transport of ions across the aqueous-organic interface. A biphasic solvent extraction system is used for this study with the organo-phosphoric acid extractant bis(2-ethylhexyl) phosphoric acid (HDEHP) dissolved in *n*-dodecane in contact with aqueous solutions of metal chlorides that contain mostly trivalent metals. HDEHP is an industrial extractant utilized for the purification of rare earth elements (REE) and the reprocessing and recycling of nuclear fuel, including its use in the TALSPEAK process (31). It is soluble in *n*-dodecane at molar quantities and in water at the submillimolar level (32). The observed precipitation removes ions and extractants from the aqueous phase; even an aqueous phase with a low solubility for extractants can act as a conduit for the transport of extractants from the organic to the precipitate phase.

Prior to undertaking these studies, we expected that a relatively high concentration organic phase of HDEHP (200 mM) placed in contact with an aqueous phase would lead merely to a rapid saturation of HDEHP in the aqueous phase at the known value of roughly 0.3 mM (20, 32). Unexpectedly, we found that quiescent biphasic solutions, apparently approaching equilibrium after the organic and aqueous phases were placed in contact, produced a precipitation front in the aqueous phase that was separated from the organic–aqueous interface by a region depleted of precipitate. Although this precipitate is soluble in the organic phase, it does not just dissolve in the organic phase because it formed away from the interface and is therefore not in contact with the organic phase. Instead, it settles to the bottom of the sample cell in the aqueous phase. The presence of ions in the precipitate phase, in addition to their presence in the aqueous and organic phases, provides a reaction path that will need to be considered in the evaluation of solvent extraction processes. Here, we report this finding by describing the conditions to form the precipitate, the spatial and temporal evolution of the precipitate, as well as the distribution of ions and extractants, for a broad selection of trivalent ions.

Results and Discussion

Precipitation in the Aqueous Phase. Shortly after placing an *n*-dodecane solution of HDEHP into contact with an aqueous solution of $NdCl_3$, streams of precipitate are observed falling downward in the lower (aqueous) phase (Fig. 1*A*; photos are colorized to enhance the observation of precipitate). The streams form earliest in samples at lower concentrations of $NdCl_3$. In the highest concentration sample, 2.0 mM $NdCl_3$, streaming is not observed even after 60 min, though precipitate formation is observed close to the interface. The last column of the photo matrix in Fig. 1 shows samples observed after 48 h which reveal precipitate that has fallen to the bottom of the sample vial in an amount that increases with the initial concentration of $NdCl_3$ (*SI Appendix*, Table S1). The precipitate appears to be fluffy in samples with a higher initial concentration of $NdCl_3$.

Analysis of the aqueous and organic phases of 48-h samples by inductively coupled plasma optical emission spectroscopy (ICP-OES) reveals that Nd has partitioned almost entirely into either the dodecane phase or into the precipitate; a negligible amount (<1 μM) is found dissolved in the aqueous phase (*Materials and Methods*). Fig. 1*B* shows that Nd is found mostly in the precipitate in samples of lower initial $NdCl_3$ concentration but is found mostly in the organic phase in samples of higher initial concentration. Therefore, the transport of Nd through the interface into the organic phase is the dominant process when the initial $NdCl_3$ concentration is larger than a cross-over value between 0.1 mM and 0.5 mM, whereas precipitation dominates when the $NdCl_3$ concentration is less than this cross-over value.

Fig. 1*C* shows that similar results are obtained when $ErCl_3$ is substituted for $NdCl_3$ (see *SI Appendix*, Fig. S4, for photos of the temporal evolution of these samples). Fig. 1 *D* and *E* show the percentage of metal ion in the precipitate for $NdCl_3$ and $ErCl_3$ samples as well as for a 1:1 $NdCl_3$:$ErCl_3$ mixture with the same total metal content and the same pH of 4.5 (*SI Appendix*, Fig. S5 for photos). Results for pH 3.0 are provided in *SI Appendix*, Figs. S6–S9. All samples show a similar qualitative behavior, though the mixed samples show that Er outcompetes Nd for precipitation in the mixed samples. This is consistent with the stronger interaction of Er with deprotonated HDEHP in the aqueous phase, as demonstrated previously (18). The amount of Er and Nd in the precipitates after 48 h is shown in *SI Appendix*, Table S1 and the amount of HDEHP is shown in *SI Appendix*, Table S2.

Interfacial Processes. The partitioning of Nd and Er into the organic and precipitate phases is the result of the two competing processes illustrated in Fig. 2*A*. In Process 1, trivalent lanthanides are transported from the aqueous to the organic phase by solvent extraction via HDEHP, which acts as an extractant to assist the transport of ions across the liquid–liquid interface (33). In Process 2, the formation of precipitate in the aqueous phase is enabled by the slight aqueous solubility of HDEHP which allows HDEHP to cross the liquid–liquid interface to dissolve in water and complex with the lanthanide ions (18, 34).

Evidence for this view of the precipitation is threefold, which includes the measured presence of HDEHP and rare earth ions in the precipitate, the reduced importance of precipitation when the aqueous solubility of HDEHP is reduced by lowering the pH, and an increase in the amount of precipitate when the organic concentration of HDEHP is increased. First, extended X-ray absorption fine structure spectroscopy (EXAFS) measurements of the precipitate reveal the presence of HDEHP and REE, at roughly

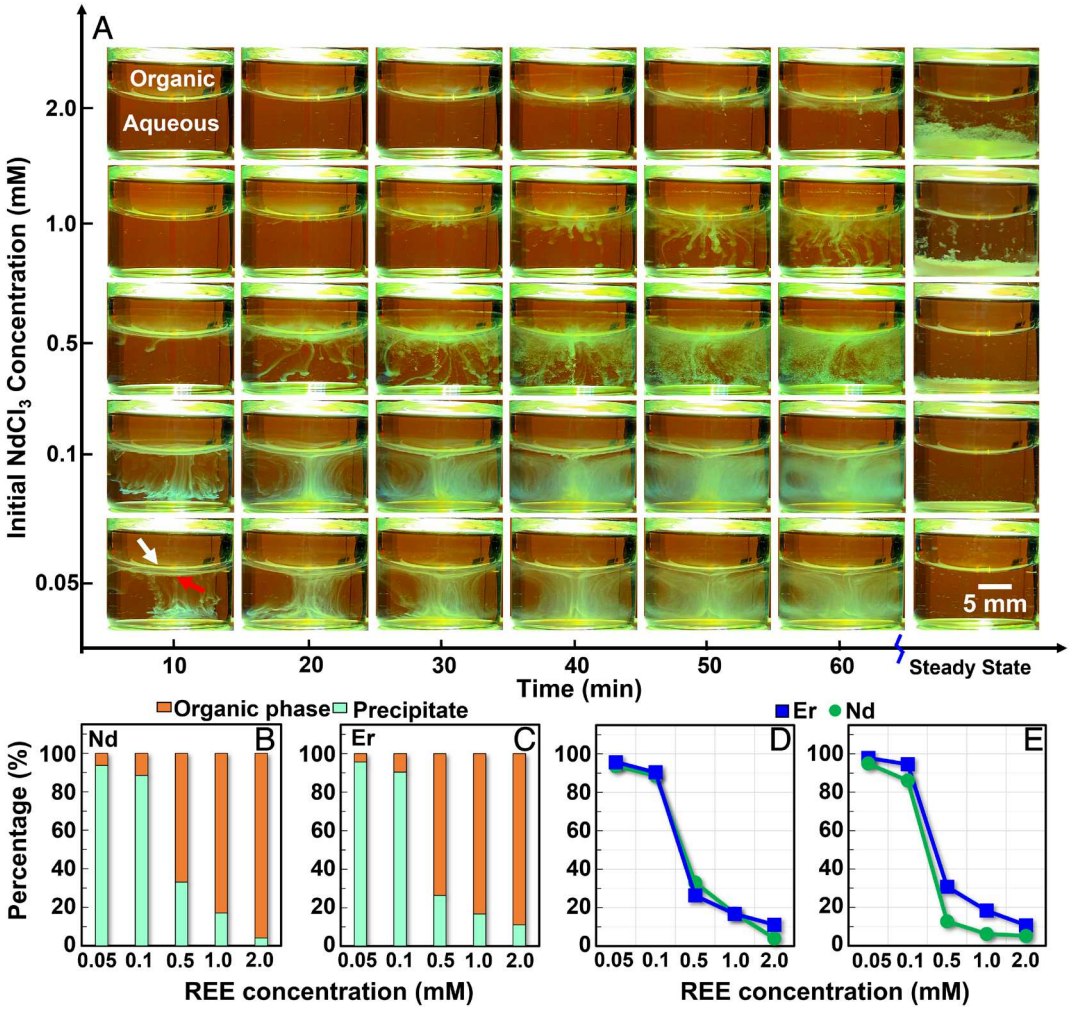

Fig. 1. Observations of liquid–liquid samples that contain initially 0.2 M HDEHP in *n*-dodecane and different concentrations of $NdCl_3$ or $ErCl_3$ in water adjusted to pH 4.5 with HCl. (*A*) The matrix of pictures is organized according to the initial concentration of $NdCl_3$ in water (by row) and the time elapsed in minutes after the organic and aqueous phases were placed in contact (by column). Steady-state observations in the last column were recorded after 48 h. Photos have been colorized to turn a white precipitate green; bulk phases are otherwise colorless. An example of the true color is shown in *SI Appendix*, Fig. S3. The upwardly curved horizontal line in each photo represents the liquid–liquid interface between the upper organic phase and the lower aqueous phase (e.g., white arrow in lower left photo). The appearance of a second line below it (e.g., red arrow in lower left photo) represents a precipitation front that breaks up by precipitate streaming with time. See *SI Appendix*, Fig. S1 for the optical setup. Movies S1–S5 show the evolution process within the first hour. (*B*) Steady-state distribution of the REE Nd in the precipitate (light green) and in the organic phase (orange) measured by ICP-OES. A negligible concentration of Nd was measured in the aqueous phase. (*C*) Steady-state distribution of Er from similar experiments when $ErCl_3$ replaced $NdCl_3$. (*D*) Percentage of REE ions Nd or Er in the precipitate for different metal ion concentrations for the results shown in (*B*) and (*C*), as well as (*E*) for samples containing a 1:1 mixture of $NdCl_3$ and $ErCl_3$ with the same total concentration of metal ions as measured in single metal component samples.

three HDEHP-$DEHP^-$ pairs per lanthanide. As shown in *SI Appendix*, Fig. S11 and Table S3, analysis of the EXAFS data shows that the coordination number of P and O about the rare earth metal ion, as well as their radial distances from the metal ion, are consistent with HDEHP-rare earth complexation observed previously (35).

Second, the amount of precipitation is reduced when the aqueous concentration of HDEHP is reduced. HDEHP is weakly soluble in water (~300 μM at pH 3.4) and has a pKa of 3.24 (36). The solubility is due primarily to deprotonated HDEHP, that is, $DEHP^-$, dissolving in water. Reducing the pH of the aqueous phase from 4.5 (above the pKa) to 3.0 (below the pKa) greatly reduces the concentration of HDEHP in water, where we use the term "HDEHP" to refer to both the protonated and deprotonated species. Visual observation of Fig. 2 *B* and *C* shows that less precipitation is present in the sample with lower pH (see *SI Appendix*, Figs. S6–S8 for the temporal evolution of pH 3.0 samples). The column figures in panels 2 *B* and *C* also show that a much lower fraction of Nd is found in the precipitates formed in lower pH samples upon achieving a steady state, which is consistent with reduced precipitation in the lower pH samples.

Third, increasing the concentration of HDEHP in the organic phase increases the amount of precipitate formed in the steady-state samples, as shown in Fig. 2 *D* and *E*, respectively, for Nd and Er. If precipitation did not occur in the aqueous phase, then increasing the HDEHP concentration in the organic phase should only reduce the time to saturate the aqueous phase with HDEHP. However, precipitation removes HDEHP from the aqueous phase. Therefore, a high concentration of HDEHP in the organic phase acts as a reservoir to supply HDEHP to the aqueous phase, which acts as a conduit, albeit of low solubility, to produce more precipitate.

Precipitation Front and Depletion Region. The two processes illustrated in Fig. 2*A* compete for HDEHP from the same source, but they do not occur at the same location in the sample. Optical microscopy of the precipitation process occurring in thin film

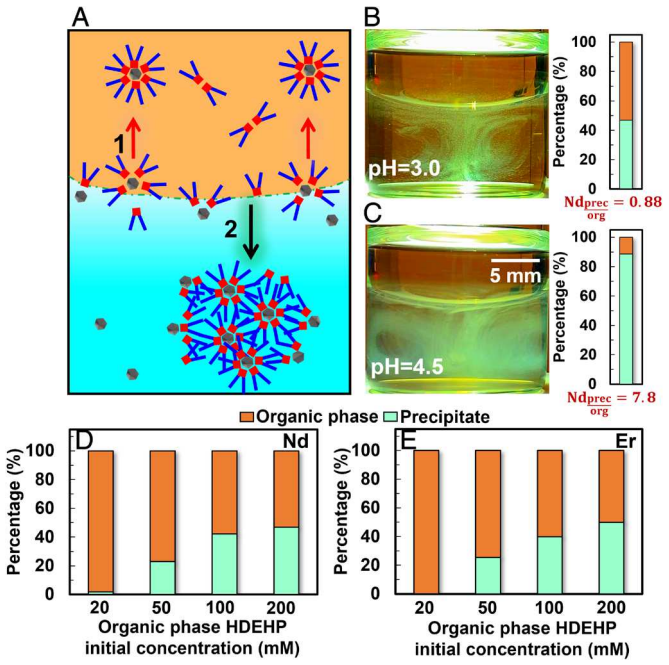

Fig. 2. Aqueous pH and organic phase HDEHP concentration alter the relative importance of the two transport processes shown in (*A*): (1) rare earth ions and HDEHP extractants interact at the interface and are transported into the organic phase, and (2) HDEHP dissolves in the aqueous phase and then forms precipitates with rare earth ions that fall to the bottom of the sample cell. Note that the structure of the aggregate/precipitate is unknown, and the cartoon is for illustrative purposes only. (*B* and *C*) Colorized photos of samples of 0.2 M HDEHP in dodecane placed in contact for 60 min with aqueous solutions of initial concentration 0.1 mM $NdCl_3$ and initial values of (*B*) pH 3.0 and (*C*) pH 4.5, along with accompanying column figure distributions of Nd in the precipitate (light green) and organic phase (orange) in the steady state after 48 h. $Nd_{prec/org}$ is the ratio of the fraction of Nd in the precipitate to fraction of Nd in the organic phase. Photos have been colorized as in Fig. 1. (*D* and *E*) Variation of lanthanide distribution with initial concentration of HDEHP in dodecane for equilibrated samples at aqueous pH 3.0 with (*D*) 0.1 mM Nd and (*E*) 0.1 mM Er, where the precipitate is in light green and the organic phase in orange. Results for mixtures of Er and Nd are shown in *SI Appendix*, Fig. S10.

samples (Fig. 3*A*) revealed a precipitation front separated by a depletion region from the liquid–liquid interface (Fig. 3*B*). The front broadens as it moves away from the interface. This precipitation front was also observed at lower spatial resolution in Fig. 1*A* as a line below the interface, which for lower concentrations (0.05 mM and 0.1 mM) was eventually swept downward by convection. The existence of the precipitate depletion region near the interface, defined as a region free of optically observable precipitates, suggests that some time is required for enough HDEHP molecules to interact with rare earth ions in the aqueous phase before HDEHP-rare earth molecular complexes become visible precipitates. During this time before visible precipitation, molecular complexes of HDEHP and rare earth ions are transported through the aqueous depletion region adjacent to the interface. This process can be represented schematically as follows,

$$\begin{aligned}&(\mathrm{HDEHP})_{org} \rightarrow \left(\mathrm{H^{+}DEHP^{-}}\right)_{aq}\\ &\rightarrow \left\{(\mathrm{DEHP^{-}})_{\mathrm{n},aq}\left(\mathrm{RE^{3+}}\right)_{\mathrm{m},aq}\right\}_{dep}\\ &\rightarrow \left\{(\mathrm{DEHP^{-}})_{\mathrm{n}',aq}\left(\mathrm{RE^{3+}}\right)_{\mathrm{m}',aq}\right\}_{prec},\end{aligned}$$

where the first step refers to transport of HDEHP from the organic to the aqueous phase, *org* and *aq* refer to species in the organic and aqueous phases, RE is a rare earth element, *dep* refers to soluble molecular complexes in the aqueous depletion region with stoichiometry "*n*" and "*m*," and *prec* refers to visible precipitation in the aqueous phase with stoichiometry "*n′*" and "*m′*." Consistent with this explanation, the depletion region is much thinner for a larger $NdCl_3$ concentration, as illustrated in Fig. 3*C*, because a greater number of ions close to the interface will be available to bind to HDEHP and form visible precipitates.

HDEHP does not extend below the precipitation front in the aqueous phase. This could be easily observed in 2 mM $NdCl_3$ samples in vials because the development of the precipitation front and precipitate streaming to the bottom of the vial takes a relatively long time, as shown in Fig. 1*A*. The Fourier-transform infrared spectroscopy (FTIR) measurements shown in Fig. 3*E* were measured on aliquots drawn from below the precipitation front (Fig. 3*D*). The absence of HDEHP below the precipitation front is indicated by the absence of P=O and alkyl chain peaks in the spectral regions, respectively, of 900 to 1,200 cm^{-1} and 2,800 to 3,000 cm^{-1}. For comparison, FTIR measurements on aliquots of the organic, aqueous, and precipitate phases of a steady-state sample are shown in Fig. 3*F*. These indicate the presence of HDEHP in all three phases in the steady state, though to a lesser extent in the aqueous phase.

Fig. 3*G* shows UV-Vis spectroscopic measurements of the Nd concentration at two locations above and below the interface, but near to it, as well as one location near the bottom of the sample vial. For this 2 mM $NdCl_3$ sample, the precipitation front passes into the region near, but below, the interface at roughly an hour of contact but precipitate does not reach the region near the bottom of the sample vial for several hours. Fig. 3*G* shows that the Nd concentration is reduced almost immediately in both aqueous regions, though the reduction in the region near the interface is faster. Fig. 3*G* also shows a corresponding fast increase in Nd just above the interface in the organic phase. The extraction of Nd from the aqueous into the organic phase leads to a removal of Nd from throughout the aqueous phase, including regions below the precipitation front which do not contain HDEHP. Eventually, the precipitation front passes through the region indicated by the magenta box in Fig. 3*G*, and later, precipitate collects at the bottom of the sample cell and Nd ions in the precipitate contribute to the UV-Vis signal from the blue box in Fig. 3*G*. The two processes illustrated in Fig. 2*A* have contributed to the concentration measurements in Fig. 3*G*. Nd ions are removed from the aqueous phase by solvent extraction across the liquid–liquid interface and transported into the organic phase (Process 1 in Fig. 2*A*), as well as the precipitation of Process 2 (in Fig. 2*A*) that collects near the bottom of the vial as shown in Fig. 1*A* for the 2 mM $NdCl_3$ sample.

Mechanistic Considerations. Two processes compete for lanthanide ions: precipitation in the aqueous phase and extraction into the organic phase. The organic phase is a source of $DEHP^{-}$ flux transported across the flat liquid–liquid interface into the aqueous precipitate depletion region. A Nd^{3+} ion that diffuses in this region can diffuse to the interface, bind with interfacial $DEHP^{-}$, and be extracted. Or it can diffuse to a $DEHP^{-}$ in the precipitate depletion region and bind to it (37), forming a complex that may eventually become part of a precipitate. Or it can diffuse to a location in which neither binding event happens.

The Nd^{3+} ions nearest the interface will have to diffuse an average shortest distance to reach the interface that is proportional to the average distance between Nd^{3+} ions in the precipitate depletion region. If [X] represents the concentration of species X, then this average distance is proportional to the inverse cube root of the Nd^{3+} concentration, $[Nd^{3+}]^{-1/3}$. If Nd^{3+} has a low concentration,

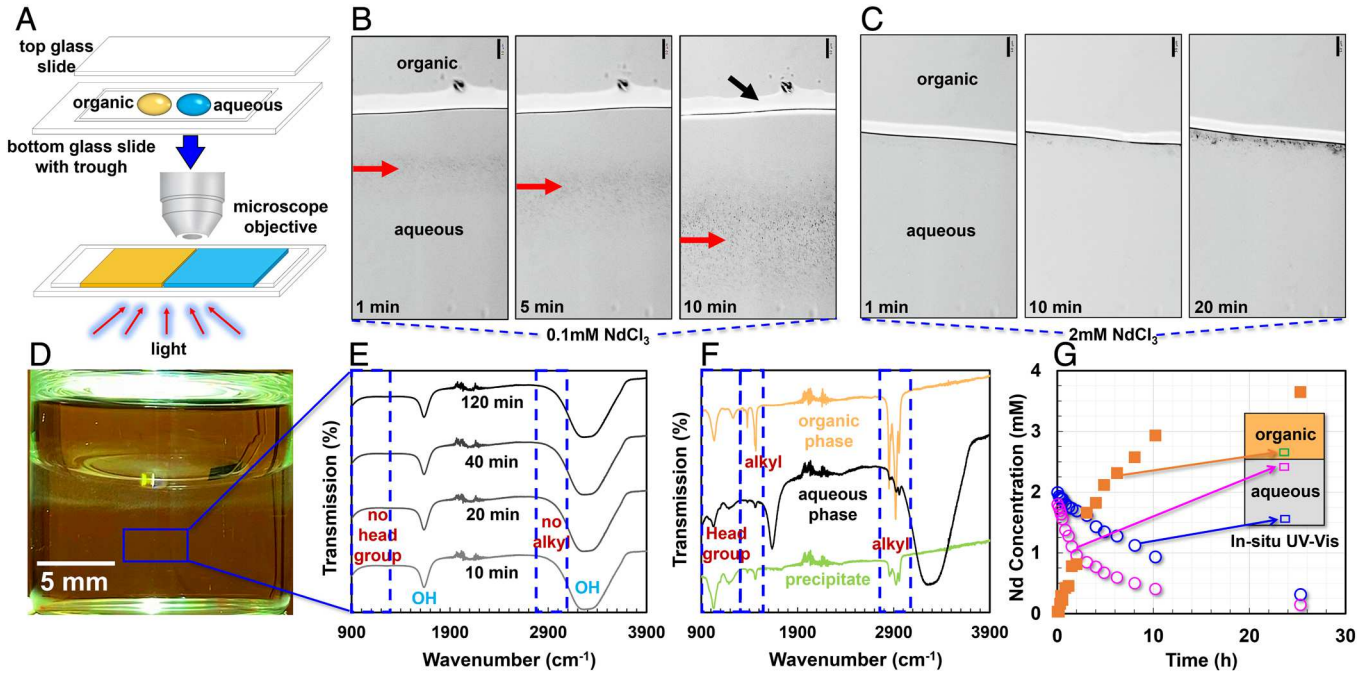

Fig. 3. (*A*) Illustration of setup for optical microscopy of thin film liquid–liquid interfaces and (*B* and *C*) corresponding images of precipitate formation between 0.2 M HDEHP in dodecane and $NdCl_3$ in water with pH of 4.5 at concentrations of (*B*) 0.1 mM $NdCl_3$ and (*C*) 2 mM $NdCl_3$, where the vertical scale bars are 50 μm long. Small black dots represent the precipitate (red arrows), and the nearly horizontal solid black line is the interface (black arrow), whereas the broad white streak above it is an optical artifact. Movie S6 shows the temporal evolution for the first 10 min. (*D*–*G*) Measurements of samples in vials containing 0.2 M HDEHP in dodecane and 2 mM $NdCl_3$ in water at pH 3.0. (*D*) The box indicates a sampling region below the precipitation front at 120 min after sample formation. (*E*) IR spectra of aliquots taken below the precipitation front at different elapsed times after placing the organic phase in contact with the aqueous phase. (*F*) IR spectra from a sample at 48 h from aliquots taken from the aqueous, organic, and precipitate phases. (*G*) In-situ UV-Vis spectroscopy of the variation of Nd concentration with time (in hours) at two locations below the precipitation front in the water phase, near (magenta) and far (blue) from the interface, as well as one location just above the interface in the organic phase. The beam is 2 x 2 mm^2. The regions near the interface are centered 2 mm below and above it, and the far region is centered 2 mm above the bottom of the sample vial. See *SI Appendix*, Fig. S2 for experimental setup. *SI Appendix*, Fig. S12 illustrates a good agreement between UV-Vis spectra and ICP measurements.

say $[Nd^{3+}] \ll [DEHP^-]$, then this average shortest distance to the interface will be much larger than the average shortest distance that Nd^{3+} will need to diffuse to $DEHP^-$ in the depletion region, which will be proportional to $[DEHP^-]^{-1/3}$. However, at higher Nd^{3+} concentrations, say $[Nd^{3+}] \gg [DEHP^-]$, these two distances will both be proportional to $[Nd^{3+}]^{-1/3}$.

This suggests that the relative probability of a Nd^{3+} binding to $DEHP^-$ in water compared to its binding to $DEHP^-$ at the interface is greater for samples with lower concentrations of Nd^{3+} than that at higher concentrations of Nd^{3+}. The cross-over concentration between these two regimes is set roughly by the concentration of $DEHP^-$ in the precipitate depletion region. If we assume that $DEHP^-$ is nearly saturated in this region, then $[DEHP^-] \approx 0.3$ mM (20, 32). This value corresponds well with the cross-over concentration at which the Nd^{3+} fraction in the precipitate varies from large to small values, as shown in Fig. 1 *B*–*E*.

This mechanism also addresses the delay in the onset of precipitation observed at higher Nd^{3+} concentrations (Fig. 1*A*). The relative probability of Nd^{3+} diffusing to interfacial $DEHP^-$ compared to Nd^{3+} diffusing to an aqueous $DEHP^-$ is higher at higher concentrations than at lower concentrations. This implies that Nd^{3+} extraction into the organic phase will be the dominant process at high Nd^{3+} concentration, as observed, which can lead to a delay in the onset of precipitation. The ongoing extraction of Nd^{3+} into the organic phase will eventually reduce the aqueous phase concentration and precipitation will become more favorable. Consistent with this, Fig. 3*G* shows that the concentration of Nd^{3+} near the interface dropped rapidly after the aqueous and organic phases were placed in contact, well before precipitate started to form in this high concentration (2 mM) sample.

Related considerations apply to the effect of changing the aqueous pH or the HDEHP concentration in the organic phase. The same logic applies to the variation of aqueous pH because an increase in pH from 3.0 to 4.5 will increase the solubility of HDEHP in water. Therefore, the relative likelihood of Nd^{3+} diffusing to $DEHP^-$ in water increases, and we expect to find that a higher fraction of Nd^{3+} precipitates in pH 4.5 samples, as observed in Fig. 2 *B* and *C*. Increasing the HDEHP concentration in the organic phase leads to a higher osmotic pressure to transport $DEHP^-$ into the aqueous phase, which either increases the $DEHP^-$ concentration in the precipitate depletion region or maintains it near the saturation value for a longer period of time. In both cases, the fraction of Nd^{3+} that forms precipitate should increase with increasing HDEHP concentration in the organic phase, as observed in Fig. 2 *D* and *E*.

Once Nd^{3+} binds to $DEHP^-$ in the precipitate depletion region, advection of the bound complex in the direction (downward) of $DEHP^-$ flux allows it to further interact with other $DEHP^-$ and Nd^{3+} to form precipitates. This leads to the precipitation front observed in Fig. 3*B* and a range of nondiffusive dynamics appears, as illustrated in Fig. 1*A*. Convective vortical structures are observed at lower concentrations of Nd^{3+} (0.05 and 0.1 mM). Although classical Rayleigh–Bénard convection is driven by a temperature gradient, an energy imbalance can produce the vortical structures in the bulk associated with this fluid instability (38). In our experiments, quasi-Rayleigh–Bénard

vortical structures appear at roughly 20 to 30 min and are fully developed at 60 min. Their generation requires both heat and mass transport (38). Heat transport is likely due to the heat released upon binding Nd^{3+} to $DEHP^{-}$ and the mass transport is due to gravity acting on the precipitate which is denser than the aqueous phase.

Quasi-Rayleigh–Taylor structures are observed at the midrange concentration levels in Fig. 1*A*. Rayleigh–Taylor fingers are observed in the 0.5 mM and 1 mM samples. Although classical Rayleigh–Taylor conditions occur strictly for zero mass transport across the interface, our observation of quasi-Rayleigh–Taylor behavior is consistent with the reduction in precipitate formation at these midrange concentrations for which mass transport is reduced (39).

Other Metal Ions. Measurements on a wide selection of trivalent metal ions revealed precipitation like that observed for Nd^{3+} and Er^{3+} (Fig. 4). Observations of mono- and divalent cations, along with the effect of co-anions with trivalent ions are presented in *SI Appendix*, Figs. S14–S16. The inverse linear relationship shown in Fig. 4 illustrates an increase of precipitation with binding affinity of metal ions to HDEHP. The brightness values plotted in Fig. 4 are a proxy for the amount of precipitate and $pH_{1/2}$ is the pH at which 50% of metal ions are extracted during solvent extraction with HDEHP (40–44). The value of $pH_{1/2}$ is considered to be an inverse measure of the binding affinity of metal ions with extractant; smaller values of $pH_{1/2}$ indicate an enhanced ability for the metal ion to bind to HDEHP. Not surprisingly, more precipitate forms when the binding affinity is enhanced.

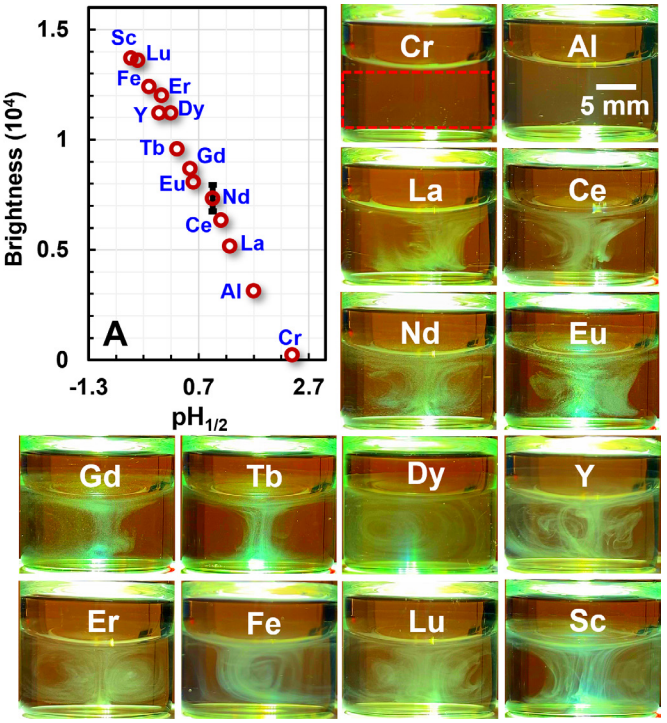

Fig. 4. Organic–aqueous samples with 0.1 mM trivalent metal chlorides at pH 3.0 with 0.2 M HDEHP in the organic phase. (*A*) Analysis of photos shown in the figure for brightness as a function of $pH_{1/2}$ values taken from the literature (see text). Photos were measured at t = 55 min after contact of the two phases. Photos have been colorized as in previous figures. Their order in the figure is according to reducing values of $pH_{1/2}$. The brightness shown in panel (*A*) was evaluated at t = 55 min after subtracting the background brightness at time t = 0. Brightness was evaluated over the region shown by the dashed red line in the Cr photo. A typical uncertainty in the brightness calculation is shown for Nd. The temporal variation of brightness for different metal ions is shown in *SI Appendix*, Fig. S17.

The Precipitate Phase Is Metastable. Complete absorption of the precipitate by the organic phase upon contact with it demonstrates that the state of these samples after 48 h, shown in Fig. 1*A*, is not the true equilibrium state. These samples contain a layer of precipitate on the bottom of the sample vial, as shown in Fig. 1*A*, indicating that it has a mass density greater than water, though it appears fluffy for higher concentration samples. Natural fluctuations of the fluffy precipitate, which bring it in contact with the dodecane phase, lead to a quick absorption and complete dissolution in the organic phase (Fig. 5*A* and Movie S7). Fig. 5*B* shows that a similar effect occurs upon shaking the sample (*SI Appendix*, Fig. S18 and Movies S8 and S9). The lipophilicity of the precipitate is consistent with the EXAFS analysis and the precipitation mechanism previously discussed which suggested that the precipitate consists mostly of HDEHP and metal ions. The solubility of the precipitate in the organic phase suggests that the precipitate depletion region is required to separate the precipitate from the organic phase and allow it to collect at the bottom of the sample vial in a metastable equilibrium. In spite of the long-lived nature of the precipitate after settling to the bottom of the aqueous phase, the sample with precipitate is in a metastable equilibrium (45). The true equilibrium state of the sample that occurs upon shaking or stirring contains only two phases—the organic and aqueous phases.

Industrial-scale solvent extraction processes utilize vats of liquids that are stirred to disperse organic phase droplets into water. High concentrations of extractants provide a strong driving force to solubilize extractant in the water even for extractants with low solubility. Below a certain value of metal ion concentration, which depends upon the extraction conditions, precipitates will form in the aqueous phase, though separated from the liquid–liquid interface by a depletion region. Such oil-drop/water/oil-drop interactions might take the form shown in Fig. 5*C* which shows precipitate forming in the water region between two convex organic phase regions in a glass tube. Stirring will bring the precipitates in direct contact with organic phase drops where they will be absorbed and dissolved, thereby transferring metal-ion-containing precipitates into the organic phase (Fig. 5 *D* and *E*).

Earlier work on the effect of aqueous complexation of HDEHP with lanthanides showed that trivalent metal ions which interacted more strongly with HDEHP were more likely to be held back in the water (18). This effect was generally antagonistic toward the intended separation because the more strongly interacting ions are expected to be preferentially extracted. The current work shows that aqueous complexation proceeds to precipitation in the presence of an organic phase reservoir that is a source of extractant. The precipitation preferentially sequesters the more strongly interacting ions in a metastable phase, the precipitate. These results emphasize a more significant role for extractants that are soluble in water, even if their solubility is low, because precipitation of HDEHP and metal ions in the aqueous phase enables the ongoing transfer of HDEHP from the organic to the aqueous phase. Competitive exchange of HDEHP and metal ions among these three phases—organic, aqueous, and precipitate—alters the traditional view of extraction kinetics, which plays an important role in designing processes to separate rare earths and other minerals.

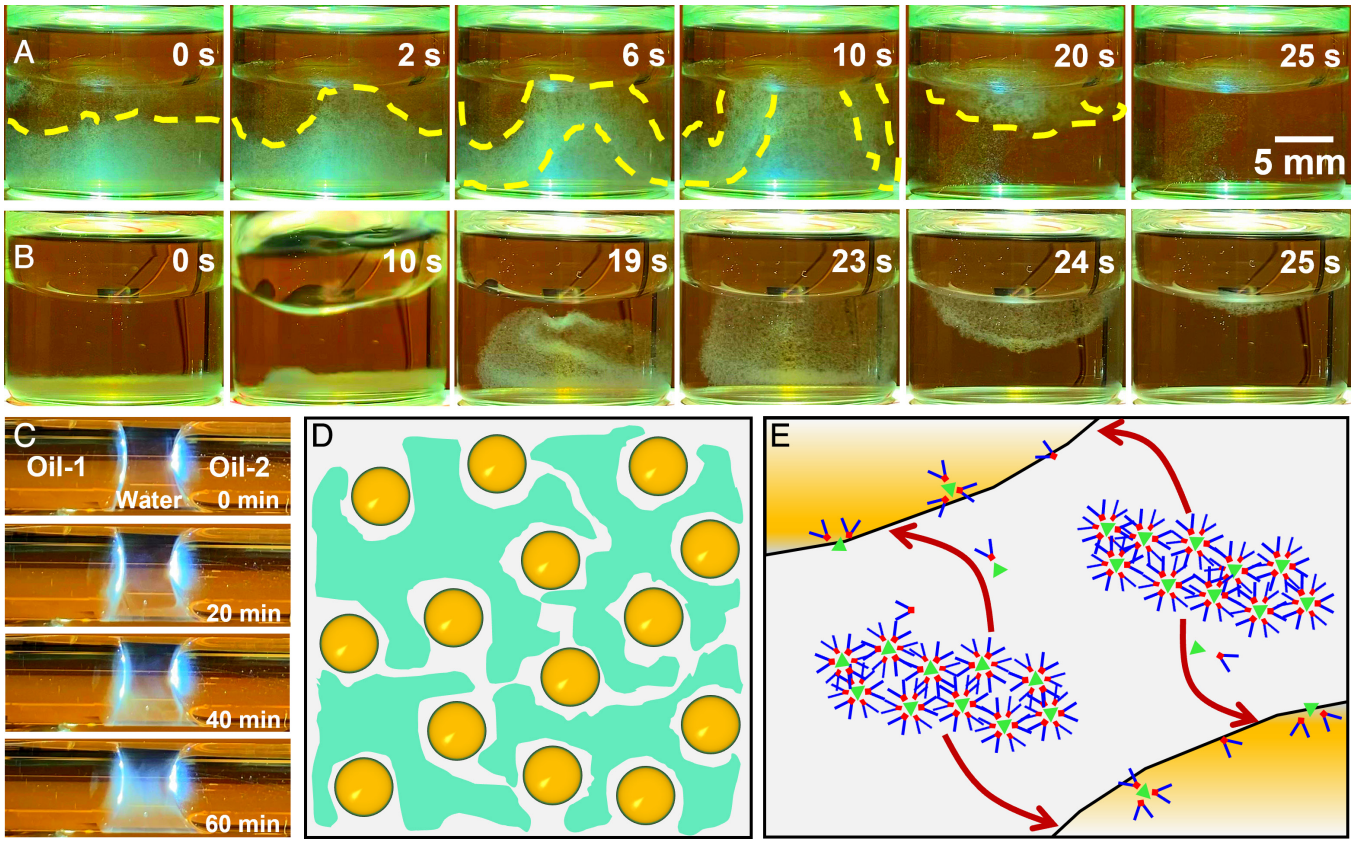

Fig. 5. Absorption and dissolution of precipitates in the organic phase. Photos have been colorized to turn a white precipitate green in (*A*) and (*B*) and light blue in (*C*); bulk phases are otherwise colorless. (*A*) Spontaneous fluctuations of precipitate in an equilibrium sample lead to its contact with the upper dodecane phase and subsequent absorption and dissolution. Yellow dashed lines are a visual guide to the precipitate motion. The initial sample composition was 0.2 M HDEHP in dodecane and 2 mM $GdCl_3$ aqueous solution at pH 3.0. Elapsed time is shown in seconds on the photos (Movie S7). (*B*) Shaken sample leads to contact of the precipitate with the upper organic phase and subsequent absorption and dissolution. The initial sample composition was 0.2 M HDEHP in dodecane and 2 mM $NdCl_3$ aqueous solution at pH 3.0. Elapsed time is shown in seconds on the photos (Movie S9). (*C*) Formation of Nd-HDEHP precipitates in the aqueous region between two convex organic phase regions that mimic two oil drops. Sample composition is 0.2 M HDEHP in dodecane and 0.1 mM $NdCl_3$ in water at pH 3.0. Elapsed time is shown in minutes on the photos (Movie S10). (*D*) Cartoon of oil drops dispersed in water during a stirred solvent extraction process (yellow balls represent oil drops; green regions represent precipitates with white depletion regions). (*E*) Cartoon of precipitate transport from water to oil drops.

Materials and Methods

Materials. Ultrapure water from a Millipore system with a resistivity of 18.2 MΩ cm was used for all aqueous solutions. Bis(2-ethylhexyl)-phosphoric acid (HDEHP, after purification, >99.9%) was purchased from Alfa-Aesar (97%) and purified via a third-phase formation procedure (46). Dodecane purchased from Sigma-Aldrich (>99%) was purified by passing it several times through activated alumina in a chromatography column to obtain a water-dodecane interfacial tension of 52 mN/m. LiCl (99.99%), NaCl(99.9%), KCl (99.9%), RbCl (99.9%), CsCl (99.9%), $MgCl_2$ (99.9%), $CaCl_2$ (99.9%), $SrCl_2$ (99.9%), $CrCl_3{\cdot}6H_2O$ (98%), $MnCl_2{\cdot}6H_2O$ (99.99%), $FeCl_3{\cdot}6H_2O$ (99.99%), $CoCl_2{\cdot}6H_2O$ (99.9%), and $NiCl_2{\cdot}6H_2O$ (99.9%), $CuCl_2$ (99.9%), $ZnCl_2$ (99.9%), $CdCl_2$ (99.9%), $PbCl_2$ (99.9%), $AlCl_3$ (99.9%), $GaCl_3$ (99.9%), $ScCl_3{\cdot}6H_2O$ (99.9%), $YCl_3{\cdot}6H_2O$ (99.9%), $CeCl_3{\cdot}6H_2O$ (99.9%), $EuCl_3{\cdot}6H_2O$ (99.9%), $TbCl_3{\cdot}6H_2O$ (99.9%), $NdCl_3{\cdot}6H_2O$ (99.9%), $ErCl_3{\cdot}6H_2O$ (99.995%), $GdCl_3{\cdot}6H_2O$ (99.99%), and $DyCl_3{\cdot}6H_2O$ (99.9%) $LuCl_3{\cdot}6H_2O$ (99.99%), were purchased from Sigma Aldrich and used without further purification. $LaCl_3{\cdot}7H_2O$ (99.99%) was purchased from Alfa-Aesar and used without further purification. Sodium hydroxide (NaOH) was purchased from Alfa-Aesar (98%) and hydrogen chloride (HCl) from Fisher Chemical (36.5 to 38.0%).

Solution Preparation. Organic solutions were prepared by dissolving purified HDEHP in dodecane (47). Stock solutions (50 mM) of metal salts were prepared with ultrapure water from a Millipore water system and then diluted to the stated concentration. The pH was adjusted with 0.01 M and 0.1 M solutions of HCl and NaOH.

Bulk Observations of Solvent Extraction. One mL of organic solution was slowly added to 2 mL of aqueous solution in a cylindrical glass vial (17 mm inner diameter). Movies were recorded at 30 frames per second for 1 h at a resolution of 1,920 × 1,080 with a smartphone camera. Longer intervals were also recorded, as shown for the 48-h measurements and in *SI Appendix*, Figs. S19 and S20. The observation in Fig. 5*C* was prepared by adding solutions in the following order: 50 μL organic solution, 50 μL aqueous solution, 50 μL organic solution, into a glass tube with an inner diameter of 4 mm to mimic an oil drop/water/oil drop arrangement.

Microscopic Observations of Thin Film Liquid–Liquid Interfaces in Fig. 3 *A* and *B*. A drop of the organic phase and a drop of the aqueous phase were placed side by side in a trough of depth 0.1 mm fabricated in a glass slide, purchased from Lianyungang Qudao Quartz Products Co., Ltd. A conventional glass slide was placed on top to flatten the drops and form a liquid–liquid interface (48). The glass slide sample cell was illuminated in transmission from below with a 12 V DC LED light source and photographed with an Olympus DP23 camera mounted on an Olympus U-TV0.63XC microscope (Japan).

Elemental Analysis. Metal ion concentrations in aliquots from the aqueous phase were measured by centrifuging an aliquot to remove solid precipitate, dilution with water, and measurement by ICP-OES. Metal ion concentrations in the organic phase were measured by stripping metal ions from an organic aliquot by a 4 M HCl aqueous solution, dilution with water, and measurement by ICP-OES. The fraction of metal ions in the precipitate was inferred from these two measurements.

Extraction Kinetics.

Ex situ measurement of kinetics by ICP-OES. Ten liquid–liquid extraction systems with the same composition (2 mL of 2 mM $NdCl_3$ in water at pH of 3.0 adjusted with HCl, and 1 mL of 0.2 M HDHEP in n-dodecane) were made at the

same time. Aliquots were withdrawn by syringe from these 10 samples, each at a different time (20 min, 40 min, 1 h, 1.5 h, 2 h, 3 h, 5 h, 10 h, 24 h, and 48 h), to measure the concentration of Nd ions (*SI Appendix*, Fig. S12). First, 600 μL of solution was removed by syringe from the organic phase near the interface, then the remaining organic phase removed by aspiration. Second, 100 μL of solution was removed by syringe from the aqueous phase near the interface. Third, 100 μL solution was removed by syringe from the bottom of the aqueous phase. Metal ion concentrations were measured as described in *Elemental Analysis*.

In-situ measurement of kinetics by UV-Vis spectroscopy. Cylindrical glass vials containing liquid–liquid samples were placed in the UV-Vis light spectroscope (Shimadzu UV2600). The height of the sample was adjusted to position the UV-Vis light beam on three different regions which corresponded to locations where aliquots were taken for ex situ measurements by ICP-OES (*SI Appendix*, Fig. S2). Spectra were measured at 2 min, 10 min, 17 min, 24 min, 31 min, 50 min, 1 h 10 min, 1 h 31 min, 2 h, 3 h 4 min, 4 h 1 min, 4 h 52 min, 6 h 12 min, 8 h 3 min, 10 h 12 min, and 25 h 18 min (*SI Appendix*, Fig. S13). *SI Appendix*, Fig. S21 shows the calibration curves for Nd in the aqueous and organic phases. *SI Appendix*, Fig. S22 shows the stability of the instrument during a long measurement.

EXAFS. Precipitates were collected from samples equilibrated for 48 h, which contained 2 mM $NdCl_3$ or 2 mM $GdCl_3$ at aqueous pH 3.0. Fluorescence EXAFS measurements from the L3-edge were measured at beamline 12-BM-B at the Advanced Photon Source (APS) of Argonne National Laboratory (49).

FTIR Spectroscopy. Aliquots were drawn by syringe from the bottom of sample vials containing 0.2 M HDEHP in dodecane and 2 mM Nd in pH 3.0 water. IR spectra of samples were measured with a Shimadzu IRTracer-100 FTIR Spectrophotometer in ATR mode with a diamond prism to detect the existence of HDEHP in the water below the precipitation front.

Brightness Calculation. The temporal evolution of precipitation formation in the aqueous phase was characterized by the brightness of photos of precipitates in the sample cell. The video was converted into individual frames in RGB format with the OpenCV python library (https://pypi.org/project/opencv-python/). Frames were converted to a grayscale format with brightness values between 0 and 1. Brightness values were summed over a selected region of interest in the aqueous phase, as shown in Fig. 4 and *SI Appendix*, Fig. S23. Background brightness at time $t = 0$, prior to forming precipitates was subtracted for Fig. 4 and *SI Appendix*, Fig. S17. Frame numbers were converted to time based on 30 frames per second.

Data, Materials, and Software Availability. All study data are included in the article and/or supporting information.

ACKNOWLEDGMENTS. This research was supported by the U.S. Department of Energy, Office of Science, Office of Basic Energy Sciences Separations Program under Award Number DE-SC0018200 to M.L.S. and from the NSF CHE-1834750 to NSF's ChemMatCARS. We thank Artem Gelis (University of Nevada at Las Vegas) for purification of HDEHP, Benjamin J. Reinhart for assistance at Sector 12 of the APS, M. Alex Brown (Argonne National Laboratory) for advice on fitting EXAFS data, and Snezhana Abarzhi for a discussion on fluid instabilities. ICP-OES measurements were performed at the Center for Nanoscale Materials, Argonne National Laboratory. Use of the APS and the Center for Nanoscale Materials, both Office of Science User Facilities operated for the U.S. Department of Energy (DOE) Office of Science by Argonne National Laboratory, was supported by the U.S. DOE under Contract No. DE-AC02-06CH11357.

Author affiliations: [a]Department of Physics, University of Illinois at Chicago, Chicago, IL 60607; [b]ChemMatCARS, Pritzker School of Molecular Engineering, University of Chicago, Chicago, IL 60637; [c]Center for Nanoscale Materials, Argonne National Laboratory, Lemont, IL 60439; and [d]Pritzker School of Molecular Engineering, University of Chicago, Chicago, IL 60637

1. J. M. Kefauver, A. B. Ward, A. Patapoutian, Discoveries in structure and physiology of mechanically activated ion channels. *Nature* **587**, 567–576 (2020).
2. B. Wei *et al.*, Influence of individual ions on oil/brine/rock interfacial interactions and oil-water flow behaviors in porous media. *Energy Fuels* **31**, 12035–12045 (2017).
3. X. Huang *et al.*, Selective recovery of rare earth elements from ion-adsorption rare earth element ores by stepwise extraction with HEH(EHP) and HDEHP. *Green Chem.* **19**, 1345–1352 (2017).
4. A. M. Wilson *et al.*, Solvent extraction: The coordination chemistry behind extractive metallurgy. *Chem. Soc. Rev.* **43**, 123–134 (2014).
5. H. Watarai, H. Freiser, Role of the interface in the extraction kinetics of zinc and nickel ions with alkyl-substituted dithizones. *J. Am. Chem. Soc.* **105**, 189–190 (2002).
6. A. G. Gaonkar, R. D. Neuman, Interfacial activity, extractant selectivity, and reversed micellization in hydrometallurgical liquid/liquid extraction systems. *J. Colloid Interface Sci.* **119**, 251–261 (1987).
7. J. Szymanowski, Kinetics and interfacial phenomena. *Solvent Extr. Ion Exch.* **18**, 729–751 (2000).
8. M. A. Hughes, V. Rod, A general model to account for the liquid/liquid kinetics of extraction of metals by organic acids. *Faraday Discuss. Chem. Soc.* **77**, 75 (1984).
9. D. B. Dreisinger, W. Charles Cooper, The kinetics of zinc, cobalt and nickel extraction in the D2EHPA-heptane-$HClO_4$ system using the rotating diffusion cell technique. *Solvent Extr. Ion Exch.* **7**, 335–360 (1989).
10. W. Bu *et al.*, Observation of a rare earth ion-extractant complex arrested at the oil-water interface during solvent extraction. *J. Phys. Chem. B* **118**, 10662–10674 (2014).
11. E. Scoppola *et al.*, Structure of a liquid/liquid interface during solvent extraction combining X-ray and neutron reflectivity measurements. *Phys. Chem. Chem. Phys.* **17**, 15093–15097 (2015).
12. Z. Liang *et al.*, A nanoscale view of assisted ion transport across the liquid-liquid interface. *Proc. Natl. Acad. Sci. U.S.A.* **116**, 18227–18232 (2019).
13. J. F. Neal *et al.*, Interfacial supramolecular structures of amphiphilic receptors drive aqueous phosphate recognition. *J. Am. Chem. Soc.* **141**, 7876–7886 (2019).
14. A. U. Chowdhury, L. Lin, B. Doughty, Hydrogen-bond-driven chemical separations: Elucidating the interfacial steps of self-assembly in solvent extraction. *ACS Appl. Mater. Interfaces* **12**, 32119–32130 (2020).
15. S. Nayak, K. Lovering, W. Bu, A. Uysal, Anions enhance rare earth adsorption at negatively charged surfaces. *J. Phys. Chem. Lett.* **11**, 4436–4442 (2020).
16. S. Nayak *et al.*, Origins of clustering of metalate-extractant complexes in liquid–liquid extraction. *ACS Appl. Mater. Interfaces* **13**, 24194–24206 (2021).
17. S. Yoo *et al.*, Specific ion effects in lanthanide-amphiphile structures at the air-water interface and their implications for selective separation. *ACS Appl. Mater. Interfaces* **14**, 7504–7512 (2022).
18. P. Sun *et al.*, Antagonistic role of aqueous complexation in the solvent extraction and separation of rare earth ions. *ACS Central Sci.* **7**, 1908–1918 (2021).
19. C. B. Honaker, H. Freiser, Kinetics of extraction of zinc dithizonate. *J. Phys. Chem.* **66**, 127–130 (2002).
20. P. Sun *et al.*, Relevance of surface adsorption and aqueous complexation for the separation of Co(II), Ni(II), and Fe(III). *J. Phys. Chem. B* **127**, 3505–3515 (2023).
21. G. Benay, G. Wipff, Liquid-liquid extraction of uranyl by TBP: The TBP and ions models and related interfacial features revisited by MD and PMF simulations. *J. Phys. Chem. B* **118**, 3133–3149 (2014).
22. W. M. Gelbart, A. Ben-Shaul, D. Roux, Eds., *Micelles, Membranes, Microemulsions, and Monolayers* (Springer-Verlag, New York, 1994).
23. R. J. Ellis, M. Audras, M. R. Antonio, Mesoscopic aspects of phase transitions in a solvent extraction system. *Langmuir* **28**, 15498–15504 (2012).
24. J. Mu, R. Motokawa, K. Akutsu, S. Nishitsuji, A. J. Masters, A novel microemulsion phase transition: Toward the elucidation of third-phase formation in spent nuclear fuel reprocessing. *J. Phys. Chem. B* **122**, 1439–1452 (2018).
25. S. Nave *et al.*, Supramolecular organisation of tri-n-butyl phosphate in organic diluent on approaching third phase transition. *Phys. Chem. Chem. Phys.* **6**, 799 (2004).
26. Y. Marcus, A. S. Kertes, *Ion Exchange and Solvent Extraction of Metal Complexes* (Wiley-Interscience, London, 1969).
27. W. Bu *et al.*, X-ray fluorescence from a model liquid/liquid solvent extraction system. *J. Appl. Phys.* **110**, 102214 (2011).
28. A. Baker, A. Fells, M. J. Carrott, C. J. Maher, B. C. Hanson, Process intensification of element extraction using centrifugal contactors in the nuclear fuel cycle. *Chem. Soc. Rev.* **51**, 3964–3999 (2022).
29. L. Berthon, A. Paquet, G. Saint-Louis, P. Guilbaud, How phase modifiers disrupt third-phase formation in solvent extraction solutions. *Solvent Extr. Ion Exch.* **39**, 204–232 (2021).
30. K. R. Swami, K. A. Venkatesan, M. P. Antony, Role of phase modifiers in controlling the third-phase formation during the solvent extraction of trivalent actinides. *Solvent Extr. Ion Exch.* **37**, 500–517 (2019).
31. K. L. Nash, The chemistry of TALSPEAK: A review of the science. *Solvent Extr. Ion Exch.* **33**, 1–55 (2014).
32. W. Su, J. Chen, Y. Jing, Aqueous partition mechanism of organophosphorus extractants in rare earths extraction. *Ind. Eng. Chem. Res.* **55**, 8424–8431 (2016).
33. T. Cheisson, E. J. Schelter, Rare earth elements: Mendeleev's bane, modern marvels. *Science* **363**, 489–493 (2019).
34. U. I. Premadasa *et al.*, Tracking molecular transport across oil/aqueous interfaces: Insight into "antagonistic" binding in solvent extraction. *J. Phys. Chem. B* **127**, 4886–4895 (2023).
35. B. J. Gullekson *et al.*, Extraction of water and speciation of trivalent lanthanides and americium in organophosphorus extractants. *Inorg. Chem.* **55**, 12675–12685 (2016).
36. K. Rama Swami, R. Kumaresan, P. K. Nayak, K. A. Venkatesan, M. P. Antony, Effect of pKa on the extraction behavior of Am(III) in organo phosphorus acid and diglycolamide solvent system. *Radiochim. Acta* **106**, 107–118 (2018).
37. Z. Liang, T. Vo, K. J. Schweighofer, I. Benjamin, M. L. Schlossman, $DEHP^-$ extractant binding to trivalent lanthanide Er^{3+}: Fast binding accompanied by concerted angular motions of hydration water. *J. Chem. Phys.* **158**, 134715 (2023).
38. S. I. Abarzhi, D. V. Ilyin, W. A. Goddard III, S. I. Anisimov, Interface dynamics: Mechanisms of stabilization and destabilization and structure of flow fields. *Proc. Nat. Acad. Sci. U.S.A.* **116**, 18218–18226 (2019).
39. S. I. Abarzhi, A. K. Bhowmick, A. Naveh, W. D. Arnett, Supernova, nuclear synthesis, fluid instabilities, and interfacial mixing. *Proc. Nat. Acad. Sci. U.S.A.* **116**, 18184–18192 (2019).
40. T. B. Pierce, P. F. Peck, The extraction of the lanthanide elements from perchloric acid by di-(2-ethylhexyl) hydrogen phosphate. *Analyst* **88**, 217–221 (1963).

41. K. C. Nathsarma, K. Sarangi, A. Mohanty, N. Devi, Liquid–liquid extraction of aluminum(III) from sulphate solution by using saponified D2EHPA. *Mater. Today: Proc.* **67**, 1185–1189 (2022).
42. N. Miralles, A. M. Sastre, M. Aguilar, M. Cox, Solvent extraction of zinc(Ii) by organophosphorus acids compounds from perchlorate solutions. *Solvent Extr. Ion Exch.* **10**, 51–68 (1992).
43. F. Islam, R. K. Biswas, The solvent extraction of chromium(III) with bis-(2-ethyl hexyl) phosphoric acid in benzene and other solvents. *J. Inorg. Nucl. Chem.* **41**, 229–233 (1979).
44. K. C. Sole, "Solvent extraction in the hydrometallurgical processing and purification of metals: Process design and selected applications" in *Solvent Extraction and Liquid Membranes: Fundamentals and Applications in New Materials,* M. Aguilar, J. L. Cortina, Eds. (Taylor & Francis, CRC Press, Boca Raton, 2008).
45. R. S. Berry, S. A. Rice, J. Ross, *Physical Chemistry* (Oxford University Press, New York, 2000).
46. H. Zhengshui, P. Ying, M. Wanwu, F. Xun, Purification of organophosphorus acid extractants. *Solvent Extr. Ion Exch.* **13**, 965–976 (1995).
47. Z. S. Hu, P. Ying, W. W. Ma, X. Fu, Purification of organophosphorus acid extractants. *Solvent Extr. Ion Exch.* **13**, 965–976 (1995).
48. G. S. Colón-Quintana, T. B. Clarke, J. E. Dick, Interfacial solute flux promotes emulsification at the water|oil interface. *Nat. Commun.* **14**, 705 (2023).
49. N. Danilovic *et al.*, Using surface segregation to design stable Ru-Ir oxides for the oxygen evolution reaction in acidic environments. *Angew. Chem. Int. Ed. Engl.* **53**, 14016–14021 (2014).